Characteristics of Reversed Propagations Generated Using Time Reversal Mirrors and Instantaneous Time Mirrors in Electromagnetics

Crystal T. Wu, Nuno M. Nobre, Emmanuel Fort, Graham D. Riley, and Fumie Costen

Abstract – The possibility of instantaneous time mirrors is explored in electromagnetic waves through the manipulation of a medium's complex relative permittivity, causing a sudden disruption to the waves' speed. The quality of the reversed foci obtained through instantaneous time mirrors and its classical alternative, time reversal mirrors, is reported in both air and water. We show how careful setup of both techniques can produce similar results. We adopt a visually guided qualitative metric as well as quantitative metrics to describe accuracy and resolution, including a newly proposed method to assess the multidimensional resolution of a focus.

1. Introduction

The principle of *time reversal invariance* allows a physical process to flow in both positive and negative temporal directions [1]. This can be thought of as if time were going backwards, akin to a video being played backwards. The process of time reversal in physical waves was shown to be possible by introducing a disruption in time or space [2]. The usual approach is through the use of a *time reversal mirror* (TRM) [3]. TRM relies on transceivers to record the wave field on a spatial boundary, then the digitally recorded waves are time reversed and reemitted from the same spatial boundary. The alternative approach, known as an *instantaneous time mirror* (ITM) [4], manipulates a time boundary to create time-reversed propagations *without* any transceivers.

The concept of ITM has been discussed theoretically [5] and tested in one-dimensional (1D) simulations for electromagnetic (EM) waves to improve fundamental understanding of temporal boundaries [6]. Practical experimentation demonstrated ITM in water waves [4], induced through a sudden change of the effective gravity, which in turn altered the waves' propagation speed. This ITM technique produced a new set of reversed wave fields that converged to the source location without using transceivers. Our work builds on the theoretical concept behind the water-based experiments in [4]. Through computer simulations, we explore the possibility of using ITM in EM waves in two dimensions via rapid manipulation of a medium's complex relative permittivity. Thus, our time-reversed waves are generated by *a change of the wave propagation speed*. In practice, one can imagine this could be achieved by rapidly modifying properties of the propagation medium, which are known to affect the electric permittivity: e.g., humidity, pressure, and temperature [7–9]. These challenges are, however, out of the scope of this paper. Instead, we focus on studying ITM theoretically in EM waves.

In theory, ITM and TRM work under the same principle but exploit different possibilities of the Cauchy initial or boundary conditions, respectively [4, 10]. Our interest here lies in the quality of the reversed foci generated by their use. Simulations of two sources placed at varying distances from each other were conducted independently in a dispersive lossy material, water, and in a nondispersive lossless material, air. Specifically, we compare results of our ITM-reversed foci to the known quality of TRM-reversed foci, produced using setups described in Section 3. In this paper, we present qualitative and quantitative evaluations of the reversed propagations generated using TRM and ITM and show how they can be carefully manipulated to closely mimic each other.

2. Analytical Metrics

Various methods have been used to describe spatial resolution. These include the following: 1D full width at half maximum (FWHM) across the target [11, 12], lateral resolution [13, 14], and the minimum size of a detectable reflective source [15, 16]. While these methods present 1D information on the resolution, resolution characteristics in other dimensions are often neglected. Here we present an additional analytic metric for spatial resolution that considers the multidimensionality of a focus.

On the basis of 1D resolution metrics, we propose multidimensional resolution to be expressed by a normalized contour plot, in which an area (or volume) can be computed based on any chosen relative intensity. Visually, the width of a peak in all directions in a space can be captured. This method allows us to relate spatial resolutions holistically in all orientations and is suitable

Manuscript received 28 August 2020.

Crystal T. Wu, Nuno M. Nobre, and Graham D. Riley are with the Department of Computer Science, University of Manchester, Oxford Road, Manchester, M13 9PL, United Kingdom; e-mail: crystal.wu@manchester.ac.uk, nunomiguel.nobre@manchester.ac.uk, graham.riley@manchester.ac.uk.

Emmanuel Fort is with the Institut Langevin, ESPCI Paris, PSL University, CNRS UMR 7587, 1 rue Jussieu, Paris, 75005, France; e-mail: emmanuel.fort@espci.fr.

Fumie Costen is with the Department of Electrical and Electronic Engineering, University of Manchester, Oxford Road, Manchester, M13 9PL, United Kingdom; e-mail: fumie.costen@manchester.ac.uk.

Table 1. Debye parameters of air [20] and water (around 30°C to 35°C [8, 9])

Material	ε_∞	ε_S	σ (S/m)	τ_D (ps)
Air	1.00	1.00	0.00	0.00
Water	74.87	5.10	0.115	6.50

for studies conducted in multidimensional spaces with a complex scenario, such as a study with a human phantom involving asymmetry and different tissues.

In this paper, the foci of reversed propagations are characterized. We explore different features of ITM and TRM and investigate the limiting distance between two sources for which the same two targets are distinguishable by the reversed waves. An example is also provided where the new multidimensional resolution analysis reveals more information than the 1D resolution metrics.

3. Multifocal Simulation Model

The point sources were each modeled as a soft source, simulating Hertzian dipole antennas [17]. The excitation current was the first derivative of a Gaussian pulse with a central frequency of 3.0 GHz, covering a range approximately from 0.1 GHz to 7.5 GHz. The two sources were identical and placed equally offset from the center of the simulation space. The TRM transceivers also implemented soft sources, but the excitation current varied depending on the experiment, as detailed below.

The numerical modeling of ITM and TRM was conducted using the transverse magnetic mode of the two-dimensional (2D) Finite Difference Time Domain (FDTD) method with a one-pole Debye model for the permittivity [17]:

$$\varepsilon_r = \varepsilon_\infty + \frac{\varepsilon_s - \varepsilon_\infty}{1 + i\omega\tau_D} - i\frac{\sigma}{\omega\varepsilon_0} \quad (1)$$

where ε_r is the complex relative permittivity, ε_∞ the optical permittivity, ε_s the static permittivity, i the imaginary unit, ω the angular frequency, τ_D the relaxation time, σ the conductivity, and ε_0 the vacuum permittivity. The simulation took place in a 1000 mm × 1000 mm space of a single medium, air or water, with absorbing boundary conditions [18]. To ensure validity of our 2D model, the temporal step Δt satisfies the stability condition in [19], given as $\Delta t \leq \delta/(v_{max}\sqrt{2})$, where δ is the length of a cell, and v_{max} the maximum wave phase velocity. Here δ is 1/10 of the minimum wavelength for numerical accuracy in the spatial derivatives [19]. For air, $\delta = 1$ mm and $\Delta t = 1.92$ ps, and for water, $\delta = 0.48$ mm and $\Delta t = 0.93$ ps. The Debye parameters used are shown in Table 1.

For TRM, the reversed propagations in air and water were induced by, respectively, 22 and 216 equally spaced transceivers surrounding the two sources. The density of transceivers was determined by the Nyquist–Shannon sampling theorem [21], corresponding to a spatial separation of half the wavelength of the central frequency. The schematic of the simulation area with the transceivers and sources is shown in Figure 1. The electric displacement field created by the initial excitation source is recorded at the transceiver locations. It can then be time reversed and introduced as the new source at the transceivers for re-emission. However, TRM is flexible in terms of manipulation of the recorded signal before re-emission. As such, we also experimented using the derivative of the time-reversed electric displacement field, the displacement current, as the new source.

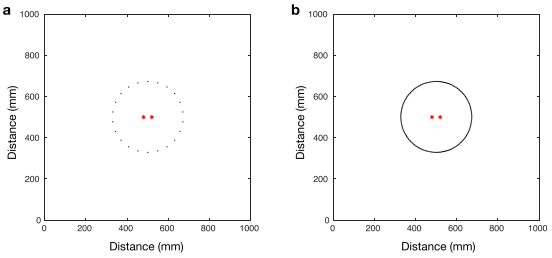

Figure 1. Arrangement of the transceivers for TRM in (a) air and (b) water are denoted by black dots. Example source locations are shown as red asterisks.

For ITM, a rapid temporal disruption of the wave speed was introduced to the entire space. We changed the phase velocity, given as $v(t) = 1/\sqrt{\varepsilon(t)\mu}$, by changing the permittivity $\varepsilon(t) = \varepsilon_0\varepsilon_r(t)$ but keeping the permeability μ constant. The disruption length affects the shape and amplitude of the reversed wave. The chosen interval is long enough so the reversed and initial waves have comparable amplitudes, while being rapid enough to mimic the effective gravity impulse discussed in [2, 4]. We linearly increased the medium's $\varepsilon_r(t)$ by 100-fold, kept it constant, then linearly returned it to its initial value. This happened over three periods of approximately 19 ps, ensuring the generated ITM time-reversed wave was the derivative of the initial forward wave field, as predicted and observed in [2, 4]. Two timings for the ITM speed disruption were studied: when all major forward waves have (1) traveled past, and (2) are passing by, the location of the TRM transceivers.

4. Analysis and Discussion

Previous research showed time-reversed waves can resolve multifocal targets, provided the distance between the sources is at least a wavelength [22]. However, the quality of the reversed wave is affected by various factors owing to the nature of TRM and ITM, whose results cannot, in general, be directly compared [2]. Despite their different nature, we show TRM transceivers can be manipulated to produce visually similar results to ITM. We also examine limitations imposed by the distance between the two sources and compare them in air and water to probe attenuation effects in TRM and ITM.

In Figures 2 to 5, numerical results of the "convergence moment" from the reversed propagations

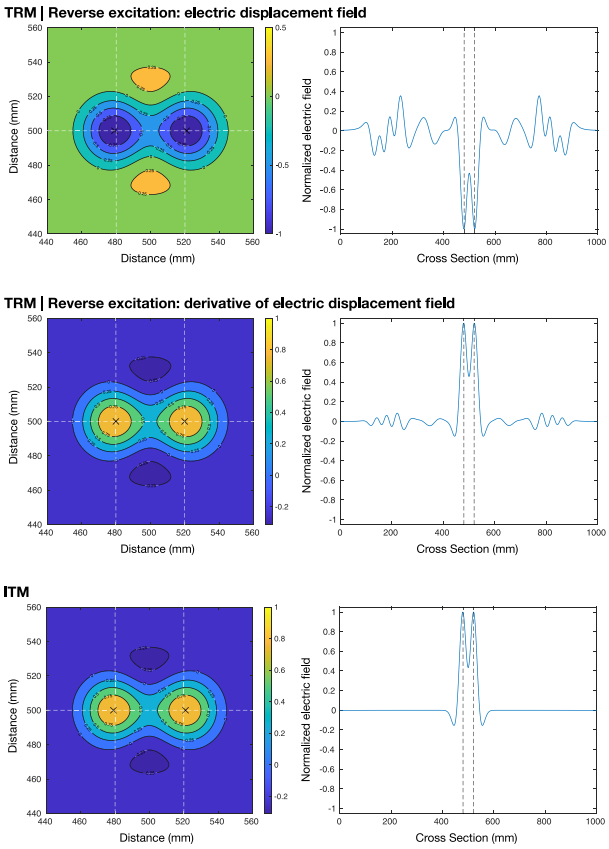

Figure 2. Multifocal target simulation in air showing TRM's reverse excitation current can be manipulated to closely reproduce ITM reverse wave fields. The sources are 40 mm apart.

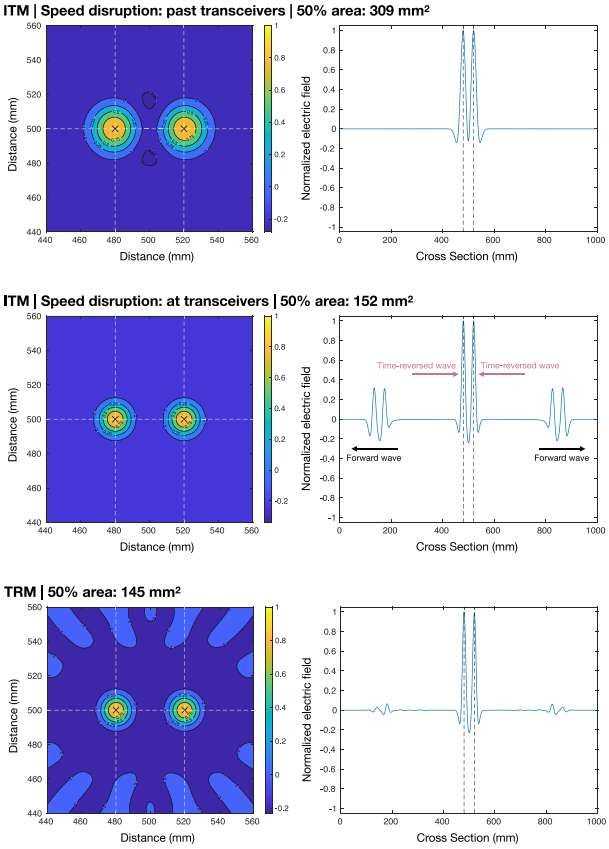

Figure 3. Multifocal target simulation in water showing ITM's disruption moment can be chosen to closely match TRM reverse wave fields. The sources are 40 mm apart.

are presented. For ITM, this moment can be approximated by doubling the time at which the speed disruption is introduced. For TRM, this would be at a time after re-emission comparable to the time it took the initial field to reach the transceivers. We define the convergence moment by looking for the least distance between the reversed foci and the targets, with the smallest 50% contour area, in a time window around the predictions above.

We report whether the reversed waves converge to distinguishable foci: qualitatively, through a 1D projection on the line passing through both sources, shown on the right of Figures 2 to 5, and quantitatively, via the 2D contour area at 50% of the peak's amplitude, on the left of Figures 2 to 5. The accuracy of the reversed foci relative to the sources' sites is also shown.

In the 2D illustrations, local maxima are denoted as black crosses, and the source locations are at the intersections of the white dashed lines. For the 1D projections, the source locations are outlined by black dashed lines. From Figure 3, the TRM results use the displacement current as the transceiver sources, and from Figure 4, ITM results use a speed disruption when the forward waves were approximately at the TRM transceiver locations.

Figures 2 and 3 present results utilizing different attributes of TRM and ITM, respectively. In Figure 2, by using the derivative of the reversed electric displacement field in TRM, the resulting reversed wave field resembles that produced in ITM. Here it is mostly a field sign issue, but we demonstrated that the collected signal can be operated on and tuned to our advantage.

Figure 3 shows the implementation time of the ITM speed disruption affects the resolution area of the 50% contour. The earlier the disruption, the smaller the area, most likely due to attenuation in water. The contour area of the TRM example provided resembles ITM, when the time of ITM disruption coincides with the distance of the TRM transceivers to the sources. Note that forward waves are also observable in some ITM results in the 1D perspective of Figures 3 and 4. Artifacts caused by the finite number of TRM transceivers are observable as well.

The quality of the reversed propagations as we vary the distance between the sources is reported under three criteria in Figures 4 and 5: (1) resolution, i.e., 2D contour area at 50% intensity of the normalized electric field, (2) accuracy, i.e., distance from reversed foci to targets, and (3) 1D qualitative observation of the two foci. We expected the two targets to be resolvable to the order of a wavelength. The wavelengths corresponding

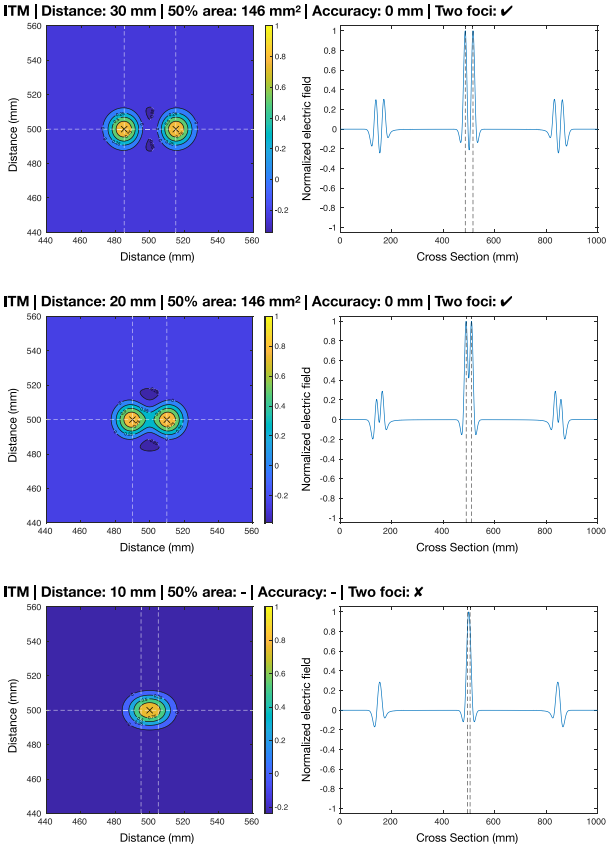

Figure 4. Multifocal target simulation in water showing ITM's resolution power for the chosen frequency range.

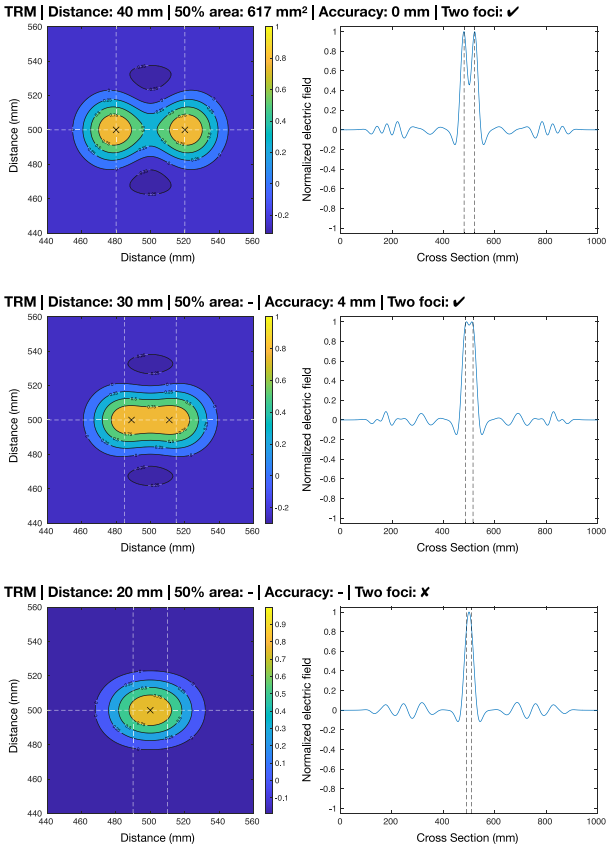

Figure 5. Multifocal target simulation in air showing the value of using multiple metrics to assess the focus quality.

to the wave's central frequency were approximately 100 mm in air and 11.6 mm in water, and 40 mm in air and 4.8 mm in water for the highest frequency, but our results suggest a limit around 30 mm to 40 mm in air and 20 mm in water for both time reversal approaches. Although the resolvable distance between the two sources is smaller in water due to the shorter wavelengths, it is higher than predicted. We believe this is caused by the loss of high-frequency components to attenuation. (Time reversal invariance is known to break in conductive lossy media [11, 12]. Compensation methods for ITM are a prospective area of research.)

In Figure 5, we compare our area-based resolution and 1D qualitative methods. For the 30 mm case, two foci can be observed in one dimension, but the 50% contour reveals inaccuracy: the two foci missed the targets and their peaks blended together. This could, however, also be seen by using the 1D FWHM. Perhaps the study of EM waves in a human phantom provides a stronger case where analysis solely from a 1D perspective may be misleading. Figure 6a is an example where the 1D FWHM in distinct orientations would be different at the convergence moment. In Figure 6b, the absolute maximum of the electric field over the whole 2D space does not fall on the target. A 1D perspective analysis would instead show a relative peak, i.e., a "false" focus. By using 2D contour graphs, we can quantify the focus area at a fraction of the absolute peak's amplitude and provide anisotropic geometrical insight.

5. Summary and Conclusion

We simulated ITM-reversed waves on a simple, symmetrical scenario, and our general observations agree with [2, 4]. We showed EM waves obtained through ITM can produce distinct foci and that, with

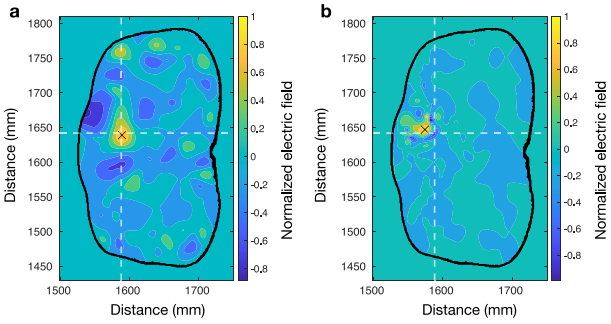

Figure 6. EM fields in a human phantom. The maximum lies on the black cross, and the source and target location where the white dashed lines meet.

manipulation, TRM can visually mimic wave fields generated by ITM even in the presence of dispersive and lossy media. We illustrated the benefits of a multidimensional resolution metric on heterogeneous media like the human body. Future work will explore attenuation-compensation methods for ITM in dispersive lossy media.

6. References

1. F. Weinert, *The Demons of Science: What They Can and Cannot Tell Us About Our World*, Cham, Switzerland, Springer, 2016, Chapter 16.
2. V. Bacot, *De certaines analogies entre le temps et l'espace pour la propagation des ondes: les miroirs et cristaux temporels*, Thèse de doctorat, Institut Langevin—Ondes et Images, Université Paris Diderot, Paris, France 2017.
3. M. Fink, "Time Reversal of Ultrasonic Fields—Part I: Basic Principles," *IEEE Transactions on Ultrasonics, Ferroelectrics, and Frequency Control*, **39**, 5, September 1992, pp. 555–566.
4. V. Bacot, M. Labousse, A. Eddi, M. Fink, and E. Fort, "Time Reversal and Holography with Spacetime Transformations," *Nature Physics*, **12**, 10, July 2016, pp. 972–977.
5. R. L. Fante, "Transmission of Electromagnetic Waves Into Time-Varying Media," *IEEE Transactions on Antennas and Propagation*, **19**, 3, May 1971, pp. 417–424.
6. Y. Xiao, D. N. Maywar, and G. P. Agrawal, "Reflection and Transmission of Electromagnetic Waves at a Temporal Boundary," *Optics Letters*, **39**, 3, February 2014, pp. 547–577.
7. A. Heidary, *A Low-Cost Universal Integrated Interface for Capactitive Sensors*, Proefschrift, Department of Microelectronics, Technische Universiteit Delft, Delft, The Netherlands, 2010.
8. T. Hermans, F. Nguyen, T. Robert, and A. Revil, "Geophysical Methods for Monitoring Temperature Changes in Shallow Low Enthalpy Geothermal Systems," *Energies*, **7**, 8, August 2014, pp. 5083–5118.
9. U. Kaatze, "Complex Permittivity of Water as a Function of Frequency and Temperature," *Journal of Chemical and Engineering Data*, **34**, 4, October 1989, pp. 371–374.
10. M. Fink and E. Fort, "From the Time-Reversal Mirror to the Instantaneous Time Mirror," *The European Physical Journal Special Topics*, **226**, 7, May 2017, pp. 1477–1486.
11. A. M. Abduljabbar, M. E. Yavuz, F. Costen, R. Himeno, and H. Yokota, "Continuous Wavelet Transform-Based Frequency Dispersion Compensation Method for Electromagnetic Time-Reversal Imaging," *IEEE Transactions on Antennas and Propagation*, **65**, 3, March 2017, pp. 1321–1329.
12. A. M. Abduljabbar, M. E. Yavuz, F. Costen, R. Himeno, and H. Yokota, "Frequency Dispersion Compensation Through Variable Window Utilization in Time-Reversal Techniques for Electromagnetic Waves," *IEEE Transactions on Antennas and Propagation*, **64**, 8, August 2016, pp. 3636–3639.
13. F. Wu, J.-L. Thomas, and M. Fink, "Time Reversal of Ultrasonic Fields—Part II: Experimental Results," *IEEE Transactions on Ultrasonics, Ferroelectrics, and Frequency Control*, **39**, 5, September 1992, pp. 567–578.
14. M. Tanter, J.-L. Thomas, and M. Fink, "Focusing and Steering through Absorbing and Aberrating Layers: Application to Ultrasonic Propagation through the skull," *The Journal of the Acoustical Society of America*, **103**, 5, May 1998, pp. 2403–2410.
15. S. Mukherjee, L. Udpa, S. Udpa, E. J. Rothwell, and Y. Deng, "A Time Reversal-Based Microwave Imaging System for Detection of Breast Tumors," *IEEE Transactions on Microwave Theory and Techniques*, **67**, 5, May 2019, pp. 2062–2075.
16. E. J. Bond, X. Li, S. C. Hagness, and B. D. Van Veen, "Microwave Imaging via Space-Time Beamforming for Early Detection of Breast Cancer," *IEEE Transactions on Antennas and Propagation*, **51**, 8, August 2003, pp. 1690–1705.
17. F. Costen, J.-P. Bérenger, and A. K. Brown, "Comparison of FDTD Hard Source With FDTD Soft Source and Accuracy Assessment in Debye Media," *IEEE Transactions on Antennas and Propagation*, **57**, 7, July 2009, pp. 2014–2022.
18. J.-P. Bérenger, "Numerical Reflection from FDTD-PMLs: A Comparison of the Split PML With the Unsplit and CFS PMLs," *IEEE Transactions on Antennas and Propagation*, **50**, 3, March 2002, pp. 258–265.
19. A. Taflove and K. R. Umashankar, "Review of FD-TD Numerical Modeling of Electromagnetic Wave Scattering and Radar Cross Section," *Proceedings of the IEEE*, **77**, 5, May 1989, pp. 682–699.
20. J. A. Huisman, W. Bouten, J. A. Vrugt, and P. A. Ferré, "Accuracy of Frequency Domain Analysis Scenarios for the Determination of Complex Dielectric Permittivity," *Water Resources Research*, **40**, 2, February 2004, pp. 1–12.
21. C. E. Shannon, "Communication in the Prescence of Noise," *Proceedings of the IEEE*, **86**, 2, February 1998, pp. 447–457.
22. S. Mukherjee, L. Udpa, S. Udpa, E. J. Rothwell, and Y. Deng, "Microwave Time-Reversal Mirror for Imaging and Hyperthermia Treatment of Breast Tumors," *Progress in Electromagnetics Research M*, **77**, December 2018, pp. 1–16.